scientific reports

Check for updates

OPEN

Investigation on optical, structural and electrical properties of solid-state polymer nanocomposites electrolyte incorporated with Ag nanoparticles

E. Salim✉, Wessam Hany, A. G. Elshahawy & A. H. Oraby

A solid polymer electrolyte based on polyvinyl alcohol (PVA)/carboxymethyl cellulose (CMC)/ polyethylene 3,4-dioxythiophene: sodium polystyrene sulfonate (PEDOT:PSS) has been prepared with various concentrations of incorporated silver (Ag) nanoparticles (NPs) by using solution cast approach. The FTIR spectroscopic study revealed the complexation between the polymeric nanocomposite (PNC) and the Ag NPs. The X-ray diffraction (XRD) results infer that the semicrystalline phase of PNC decreases as the amount of incorporated Ag NPs increases. The transmission electron microscope (TEM) image revealed that Ag NPs have diameters ranging from 22 to 43 nm. Complex dielectric permittivity and alternating current (AC) electrical conductivity of nanocomposite films have been investigated in the frequency range from 0.1 Hz to 20 MHz at 30 °C. Dc conductivity (σ_{dc}) values for the nanocomposite films are estimated from AC conductivity plots. The σ_{dc} value was observed to increase from 1.98×10^{-9} to 2.29×10^{-7} S.cm^{-1} for the PNC system incorporated with optimal Ag NPs. From complex impedance (Z*) analysis, it has been found that the bulk electrical resistance (R_b) of the PNC films decreases with increasing the Ag NPs content. Therefore, these obtained PNC films have promising applications in energy storage devices.

In recent years, the development of solid polymer electrolyte (SPE) has made great advances in sensors, high energy density batteries, electrochromic displays and windows, and photovoltaic cells due to its flexibility, electrochemical stability, long life, and safety[1,2]. Polyvinyl alcohol (PVA) has interesting characteristics and a wide range of uses. It possesses high dielectric strength, strong charge storage capacity, high elasticity, and good film formation via solution casting[3,4]. It also contains hydroxyl side groups, which can interact with a variety of substances via physical or chemical action[5]. Furthermore, Carboxymethyl cellulose (CMC), available as sodium salt NaCMC is a polyelectrolyte smart cellulose derivative, non-toxic, biodegradable, and has a large number of carboxyl groups (–COOH)[6]. So, it can create a strong connection with PVA via hydrogen bonding and subsequent cross-linking[7]. The addition of CMC to the PVA matrix can enhance the polymer's properties[8]. To impart higher conductivity to the polymer blend, conductive additives with dispersibility and good conductivity are required. A large number of π-conjugated polymers can transport electrons, so the addition of polypyrrole[9–11], polyaniline[12,13], poly (3,4-ethyldioxythiophene) polystyrene sulfonate (PEDOT:PSS)[14,15] into the polymer blend to enhance its conductivity. Among these polymers, PEDOT:PSS has high electrical conductivity (σ), excellent electrochemical stability, and film-forming capabilities. In addition, PEDOT:PSS has also been used as electrocatalysts[16], capacitors[17,18], transistors[19], solar cells[20], and sensors[21,22]. To produce nanocomposites, nanoparticles (NPs) within the polymeric blend interact and create molecular bridges. Large polymeric/nanofiller interfacial regions are formed as a result of the uniform distribution and excellent dispersion of these NPs, which improve the materials' electrical and dielectric characteristics[23]. Recently, several experiments have been performed to manufacture nanocomposite materials incorporating a variety of inorganic NPs, including zinc oxide (ZnO)[24,25], copper (Cu)[26], gold (Au)[27], and silver (Ag)[28], with different polymers. Among these inorganic NPs, Ag has the highest electrical conductivity (σ =6.3×10^5 S.cm^{-1} at 20 °C) of any metal and is relatively inexpensive compared to other noble metals[29].

Physics Department, Faculty of Science, Mansoura University, Mansoura, Egypt. ✉email: ehabahmed@mans.edu.eg

In this work, SPE-based PNC films, PVA/CMC/PEDOT:PSS/various weights Ag NPs, were prepared. XRD, FTIR, and TEM were used to examine the structural properties of the produced nanocomposite films. Moreover, the impact of the Ag NPs content on the optical, electrical and dielectric properties of the prepared films has been investigated.

Experimental details

Materials. Polyvinyl alcohol (PVA, M.W. = 89,000–98,000, 99+% hydrolyzed), Poly(2,3-dihydrothieno-1,4-dioxin)-poly(styrene sulfonate) (PEDOT:PSS, 1.3 wt% dispersion in H_2O), and carboxymethylcellulose (CMC, average M.W. = 250,000) were purchased from Sigma-Aldrich. Ag NPs (M.W. = 107.87) were purchased from Nanjing Chemical Reagent Co. Ltd. All the chemicals were analytically pure and used without purification.

Preparation of PVA/CMC/PEDOT: PSS/Ag NPs. Firstly, 1 g PVA and 0.5 g CMC were dissolved in 50 ml deionized water (DW) at 90 °C and 70 °C respectively, and then the two solutions were mixed and stirred for 3 h until completely dissolved. Secondly, five solutions of 10 ml of the above dissolved PVA/CMC and 0.3 ml of PEDOT:PSS in H_2O were taken and mixed under stirring for 1h, and then 0, 1, 3, 5, 7 mg Ag NPs dispersed in 0.5 ml DW were added and continued to stir for 1 h, respectively. Finally, the resulting solutions were poured into polystyrene Petri dishes and evaporated at 50 °C. The as-prepared films with a thickness of 10–20 microns were labeled PCPP0, PCPP1, PCPP2, PCPP3, and PCPP4 based on the amount of Ag NPs added gradually.

Characterization. X-ray diffraction (XRD) patterns of the nanocomposite films were recorded at room temperature using DIANO corporation USA with CuKα radiation in the Bragg angle $2\theta = 5°–70°$. Fourier transform infrared (FTIR 430-JASCO, Japan) spectrometer measurements were recorded within the 400–4000 cm^{-1} range. The optical absorptions of the films were obtained using a UV–visible spectrophotometer (JASCO V-630-Japan) at $\lambda = 190–900$ nm. The size of Ag NPs was investigated by transmission electron microscope (TEM, JEOL/ JEM/1011, Japan). The scanning electron microscope (SEM, JEOL-JSM 6510/LV/250, U.S.A., at magnification 6,000X) was used to investigate the surface topography. Impedance and dielectric characteristics of the PNC films were carried out in the 10^{-1} Hz–10 MHz range at room temperature (305 K) using broadband dielectric spectroscopy (Novo control Turnkey Concept 40 System).

Results and discussion

FT-IR analysis. Fourier-transformed infrared (FTIR) spectroscopy was used to investigate the chemical structure of solid films. Figure 1a shows the FTIR spectra of PVA, CMC, and PEDOT:PSS. According to the FTIR spectrum of pure PVA, there is a wide characteristic peak observed at 3450 cm^{-1} assigned to the stretching vibration of intermolecular and intramolecular –OH bonds. The peaks at 2936 and 1725 cm^{-1} pertain to the stretching vibration of C–H and carbonyl C=O groups, respectively[30,31]. Also, the noticed peaks at 1430 and 1375 cm^{-1} are assigned to the bending and wagging of CH_2 vibrations, respectively[32]. However, peaks at 1250, and 850 cm^{-1} are due to the stretching vibration of C–O and C–C groups, respectively. The above-all peaks confirm the existence of PVA. The peaks at 2914, 1630, 1413, 1323, 710, and 607 cm^{-1} are all correlated to pure CMC[33]. For PEDOT:PSS, the peak around 3400 cm^{-1} is due to the O–H stretching, the peak at 1645 cm^{-1} is due to the bending of the C=C group, peaks at 1196 and 1034 cm^{-1} are due to the stretching of C–O–C bond, and peak at 809 cm^{-1} is attributed to C–S bonds in thiophene backbone[34,35]. The characteristic peaks of PVA, CMC, and PEDOT:PSS can be noticed from the PVA/CMC/PEDOT:PSS (PCPP0) nanocomposite film, and the results of various weights of incorporated Ag NPs into PCPP in Fig1b. The oxygen-containing functional group (SO_3 $-H^+$) of PEDOT:PSS can interact and cross-link with PVA/CMC via hydrogen bonding[36,37]. With the following Ag NPs incorporating process into PCPP, the broadening and decreasing in the peak intensity suggest the physical interaction occurred between them[38].

X-ray diffraction (XRD) analysis. Figure2 shows the XRD patterns for PCPP0, PCPP1, PCPP2, PCPP3, and PCPP4 from 5° to 70°, confirming the successful complexation between PVA, CMC, and PEDOT:PSS. It have been reported that PVA, CMC, and PEDOT:PSS have diffraction peaks lying at $2\theta = 19.5°$[39], $2\theta = 20.7°$[40] and $2\theta = 25.6°$[41], respectively. It can be observed that the PCPP0 shows the existence of a semicrystalline phase with the diffraction peak centered at $2\theta = 19.3°$. This peak becomes more broadening and less intense as the Ag NPs increase which suggests the transference of PCPP from semicrystalline to amorphous structure. In addition, the higher weights of Ag NPs showed diffraction peaks at $2\theta = 38°$, $2\theta = 44°$, and $2\theta = 64°$, corresponding to (111), (200), and (220) lattice planes, respectively[42].

Optical absorption study

The optical characteristics of the nanocomposite films (PCPP0 → 4) are investigated using a UV–vis spectrophotometer in the wavelength range 190–900 nm as shown in Fig. 3. An absorption band and hump are observed for all films at about 205 and 265 nm, respectively, which are ascribed to π-π* transition[43]. It is seen that there is an increase in the absorption peaks and is red-shifted with the increase of the incorporated Ag NPs. The optical energy bandgap (E_g) of the prepared films could be obtained from the absorption spectra using Tauc's formula[44]:

$$\alpha h\upsilon = \beta\left(h\upsilon - E_g\right)^m \quad (1)$$

where α is the absorption coefficient, β is a constant, and m is an empirical index of the transition modes. To calculate the direct optical energy gap (E_g^d) for the investigated films, the quantity $(\alpha h\upsilon)^2$ is plotted as a function of photon energy ($h\upsilon$) (Fig. 4a). For undoped film PCPP0, the optical energy gap was observed to be 5.16 eV

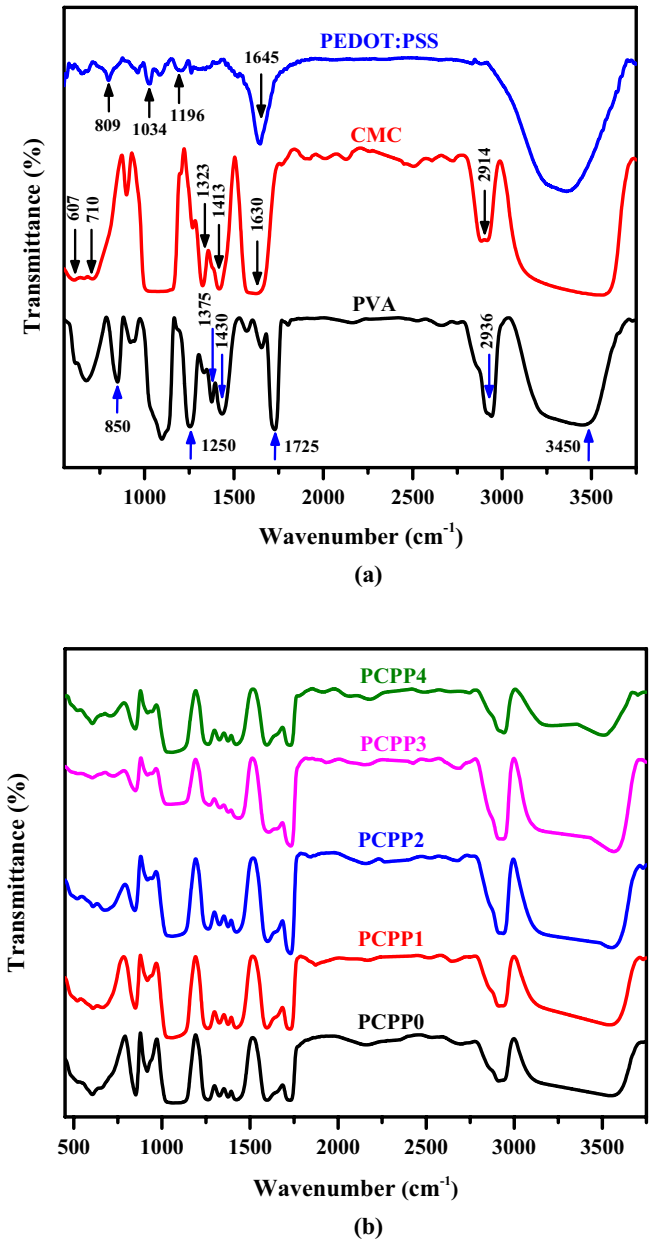

Figure 1. (**a**) FTIR spectra of PVA, CMC, PEDOT: PSS, and (**b**) PCPP with various Ag NPs weights films.

while for incorporated films PCPP1 → 4, the values were 5.15, 5.12, 5.07, and 5.01 eV, respectively. On the other hand, the indirect optical energy gap (E_g^{in}) were calculated using $(\alpha h\upsilon)^{1/2}$ versus ($h\upsilon$) plots (Fig. 4b) and found to be 4.9 eV for PCPP0 and 4.85, 4.79, 4.64, and 4.44 eV for dopped films, respectively. The values of direct and indirect optical energy gaps are listed in Table 1. It is clear that the decrease in the values of E_g^d and E_g^{in} on doping PCPP with Ag NPs may be attributed to the formation of charge-transfer complexes[45]. In addition, the enhancement in the absorption coefficient of the PNC films may be related to the agglomeration of Ag NPs, which may scatter the light within the PNC samples[46].

Transmission electron microscope (TEM). Figure 5 shows the TEM image of Ag NPs. It has a nearly spherical shape with sizes ranging from 22 to 43 nm.

Morphological studies. Scanning electron microscope (SEM) is a commonly used technique for identifying the formation and growth of agglomerated metallic NPs that leak to the surface of polymer nanocomposites[47,48]. Figure 6a–e show the surface morphology of PCPP films. From the top view of the PCPP0 nanocomposite film, the micrograph appeared to be smooth and promoted the good quality of the prepared films. When the Ag NPs content increased gradually, aggregated particles were formed, and their sizes increased. The consequences of

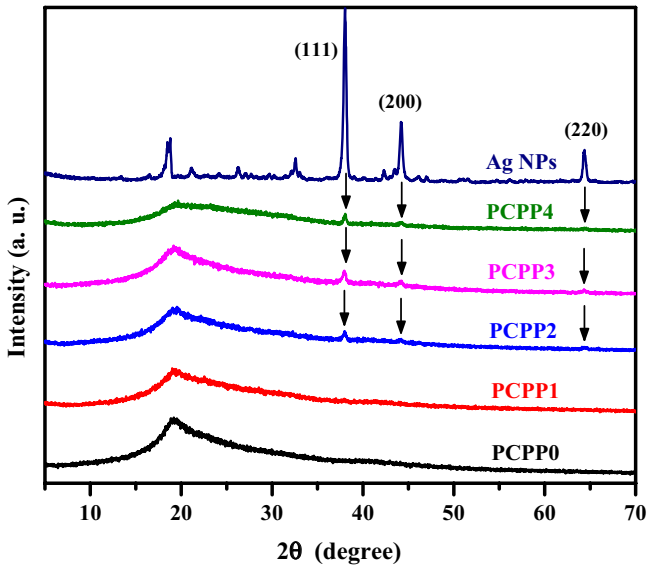

Figure 2. XRD spectra of PCMPP with various Ag NPs concentrations films.

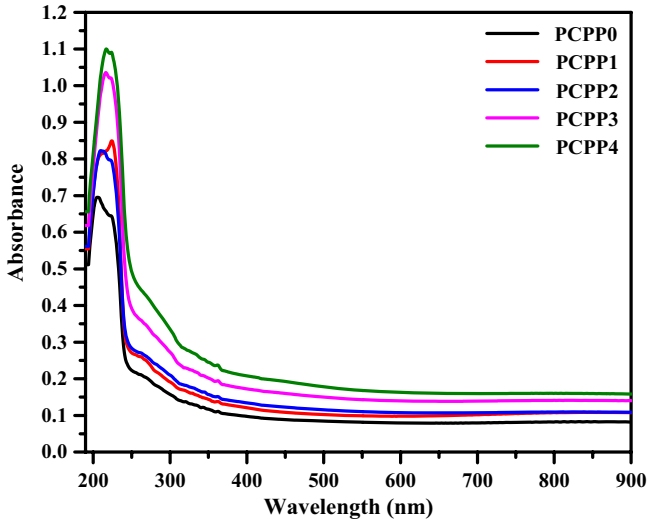

Figure 3. UV–vis absorption spectra of PVA/CMC/PEDOT: PSS with various weights of Ag NPs.

the morphological alterations were revealed in the dielectric characteristics of the nanocomposite films and are described further below.

AC conductivity. Figure 7 shows the plot of AC conductivity as a function of frequency in the range of 0.1 Hz–20 MHz at room temperature. As noted, the behavior of $\sigma_{ac}^{'}$ increases nonlinearly with increasing frequency. This can be attributed to the hopping mechanism of charge carriers that acquires by providing the electrical field which in turn increases the relaxation frequency and so enhances the conductivity[49]. It is found that the frequency-dependent spectra of the nanocomposite films exhibit three distinguished regions; (i) the low-frequency dispersion region, which is related to the accumulation of charge (electrode polarization) at the electrode/polymer interface, (ii) the mid-frequency independent plateau region, which is attributed to DC conductivity σ_{dc}, and (iii) high-frequency dispersion region which is attributed to short-range ion transport, which is caused by the charge carrier's Coulomb interaction. So, the σ_{dc} values of the films can be estimated using Jonscher's power law[50,51];

$$\sigma_{ac}^{'}(\omega) = \sigma_{dc} + A\omega^{m} \quad (2)$$

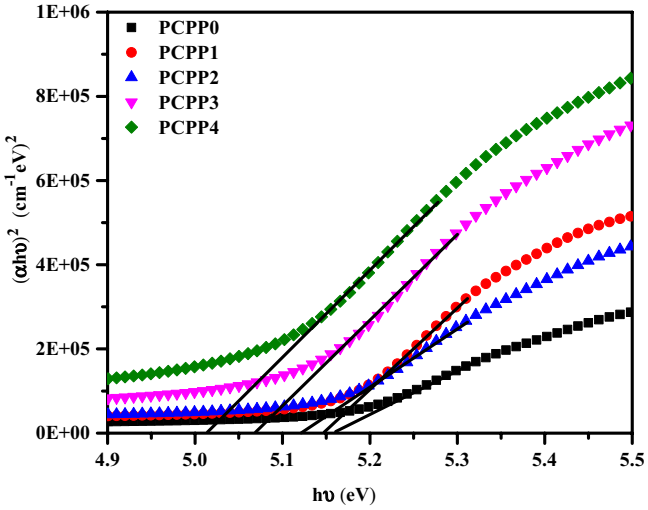

Figure 4. (**a**) $(\alpha h\upsilon)^2$ and (**b**) $(\alpha h\upsilon)^{1/2}$ versus hυ of PVA/CMC/PEDOT: PSS with various weights of Ag NPs.

Films	E_g^d(eV)	E_g^{in}(eV)
PCPP0	5.16	4.9
PCPP1	5.15	4.85
PCPP2	5.12	4.79
PCPP3	5.07	4.64
PCPP4	5.01	4.44

Table 1. The extracted values of direct and indirect energy bandgap for PVA/CMC/PEDOT: PSS with various weights of Ag NPs.

where A represents the frequency-independent pre-exponential constant, ω is the angular frequency ($\omega = 2\pi f$), and m is the power-law exponent ($0 < m < 1$). The σ_{dc} of the undoped and doped Ag NPs films has been calculated by intersecting extrapolated plateau region of $\sigma_{ac}^{'}$- axis. It is noticed that the σ_{dc} value increased from 1.98×10^{-9} to 7.41×10^{-8} S.cm^{-1} for PCPP0 and PCPP3 films, respectively. The increase in σ_{dc} values of the nanocomposite films with the increase of dispersed Ag NPs contents indicates that there is either increase in charge carrier mobility or an increase in Ag ion carriers that contribute to the conductivity and polarization mechanisms. While the

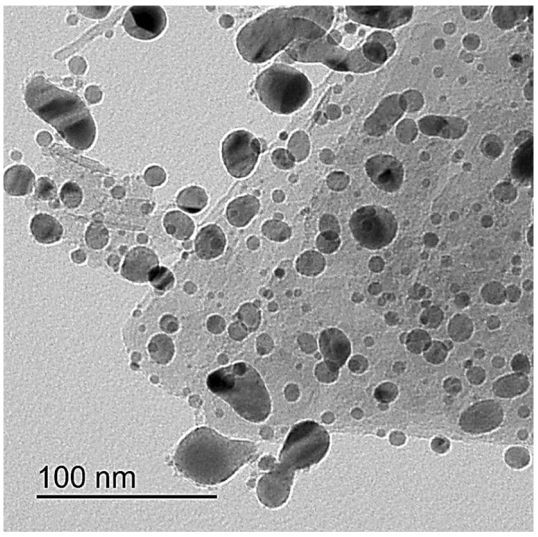

Figure 5. TEM images of Ag NPs.

higher the content of Ag NPs in the PCPP4 film, the lower the σ_{dc} value. This decrease may be attributed to the reduced Ag NPs which might act as grain boundaries and impede the Ag ion carriers to be transported through the polymeric matrices. Therefore, a few Ag ions participate in the conductivity and polarization.

Dielectric studies. It is well known that the dielectric spectroscopy of polymeric materials is a powerful technique to understand the variation of electrical conductivity mechanisms. So, the dielectric data of the nanocomposite films were analyzed using the complex dielectric constant ε^* as following[52,53]:

$$\varepsilon^* = \varepsilon' - j\varepsilon'', \ \varepsilon' = \frac{Cd}{A\varepsilon_o}, \ \varepsilon'' = \frac{\sigma_{ac}}{\varepsilon_o \omega} \tag{3}$$

where ε' is the real part of the relative permittivity (dielectric constant), ε'' is the imaginary part of the relative permittivity (dielectric loss), C is the capacitance of the film, d is the film's thickness, A is the surface area of the electrodes, and $\varepsilon_o = 8.85\ 10^{-12}$ F/m is the free space-permittivity. The ε' value measures the amount of charge that can be stored by the material, whereas the ε'' the amount of energy lost. Plots of both ε' and ε'' against log f of the nanocomposite films at room temperature are shown in Fig. 8a and b, respectively. It is seen that the behavior of ε' and ε'' increase non-linearly with the decrease in frequency at room temperature. This phenomenon is more noticeable at lower frequencies ($f < 10^2$ Hz). The increase in permittivity with the decrease of frequency indicates that the system shows interfacial polarization at a low frequency[54]. On the other hand, the response of charge carriers at low frequency is faster with an externally applied electric signal, resulting in a higher value of ε'. The values of ε' and ε'' increased with increasing Ag NPs content until PCPP3 nanocomposite film. This can be attributed to an increase in the density of Ag ion carriers as well as an increase in polarization. However, when the Ag NPs increased above the PCPP3 sample, the values of the dielectric constant and dielectric loss were reversed. This decrease in ε' and ε'' values could be related to the reduction of Ag-ion carriers to Ag particles. At high frequency, the permittivity values are found almost independent of the frequency due to the charge carriers being unable to reorient themselves with the applied electric field. Furthermore, ion oscillations may be the only source of the dielectric constant at high frequency, so ε'' is frequency independent. These results suggest that the dielectric constant might be used to evaluate the conductivity of the nanocomposite films.

Impedance analysis. Impedance spectroscopy is a well-known technique used to determine ion dynamics in polymer electrolyte systems. In the current SPE, ac impedance measurements were used to illustrate electrolyte conductivity and frequency-dependent action. The Cole–Cole plots (Nyquist plots) for nanocomposite films based on SPE at room temperature are shown in Fig. 9. The obtained complex impedance spectra show two distinct regions; the high-frequency semi-circle region, which is due to the ionic conducting nature in the bulk of the polymer electrolytes, and the low-frequency spike, which is due to the blocking electrode (space charge polarization effect)[55]. To clarify the relationship between microstructure and electrical characteristics, impedance data is often represented as an equivalent electric circuit consisting of resistance and capacitance. The impedance data were fitted with an equivalent circuit using EIS software. As shown in the inset Fig. 9a–e, this equivalent circuit of the PNC films consists of a parallel combination of resistance R_b and fractal capacity CPE1 in series with other fractal capacity CPE2. A CPE is a constant phase element that indicates a deviation from the ideal Debye-type model. R_b represents the bulk resistance in this model, and it can be calculated using the low-frequency intercept of the semi-circle on the Z′ axis. CPE1 and CPE2 are simple distributed components that provide impedance with a constant phase angle in the complex plane. The impedance of the CPE is described by the following formula:

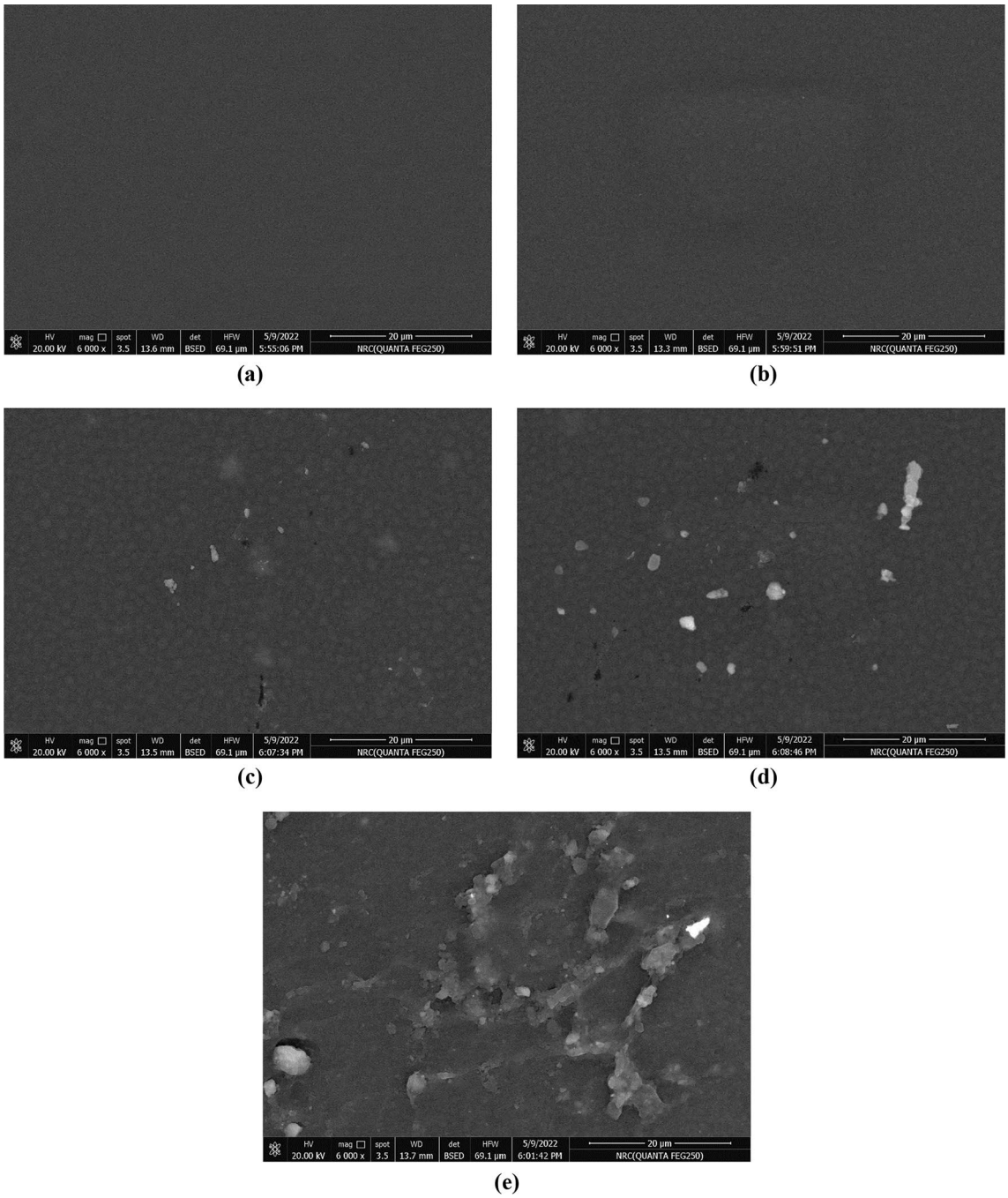

Figure 6. SEM images of (**a**) PCPP0, (**b**) PCPP1, (**c**) PCPP2, (**d**) PCPP3, and (**e**) PCPP4 at magnification 6,000 times.

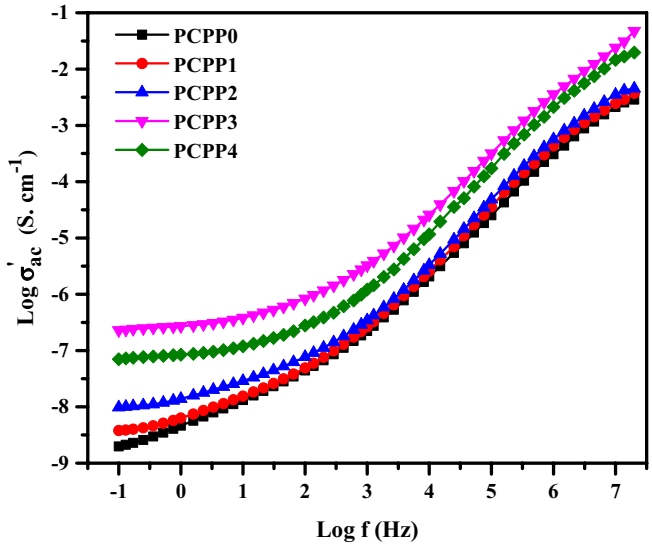

Figure 7. Log AC conductivity versus log frequency for all films at room temperature.

$$\mathrm{ZCPE} = \frac{1}{\mathrm{Q}(\mathrm{i}\omega)^{\mathrm{n}}} \tag{4}$$

where Q represents the numerical value of $1/|Z|$ at $\omega = 1$ rad s^{-1} and n represents the phase of the components, which gives the degree of deviation from the pure capacitor. The parameters of the equivalent electric circuit model are derived by fitting the curves in Fig. 9 are listed in Table 2. It can be noticed that the R_b decreases as the Ag NPs concentration increases. Also, the semi-circle centers are observed to be below the Z′- axis. This implies that the ions' relaxation in the prepared samples is non-Debye kind. The lack of a high-frequency semi-circle indicates that overall conductivity is mostly due to ion conduction[56,57].

Conclusions

In summary, we incorporated various amounts of Ag NPs into PVA/CMC/PEDOT:PSS composite to prepare the solid nanocomposite electrolyte. The solution casting approach was used to prepare the nanocomposite films, and the obtained films were physically and electrically characterized. PVA and CMC are utilized as hydrophilic structures, which provide flexibility to the films. The presence of the PEDOT:PSS provides the conductivity of the films. FT-IR spectra reveal the complex formation between the Ag NPs and PVA/CMC/PEDOT: PSS nanocomposites, and the complexation of polymers composite each other. The XRD pattern shows that the amorphous nature of the films increases with the addition of the Ag NPs, and three characteristic diffraction peaks confirmed the presence of Ag NPs. Furthermore, it was noticed that increasing the Ag NPs concentration has a significant influence on reducing the optical band gap energies. SEM images revealed the miscibility between the PVA, CMC, and PEDOT:PSS by a homogeneous smooth surface. Moreover, the surface structure of the PNC films is influenced by the Ag NPs filling ratio. The optical characteristics of the PNC films indicated that as the concentration of the Ag NPs increased, the absorbance increased while the optical band gap decreased. The AC conductivity values for the prepared films were increased up to the optimal nanocomposite film PCPP3, which can be ascribed to the increased contribution of Ag ion carriers to the conductivity and polarization mechanisms. Both ε' and ε'' also increased at the optimal nanocomposite film PCPP3 which in turn facilitates the charge carriers' mobility. Also, the reduction in the diameter of semi-circle impedance plots indicates an increase in ionic conductivity. Further addition of Ag NPs in the composite films reduced the σ_{dc}, ε', and ε'' due to the increase in the rate of Ag ion reduction.

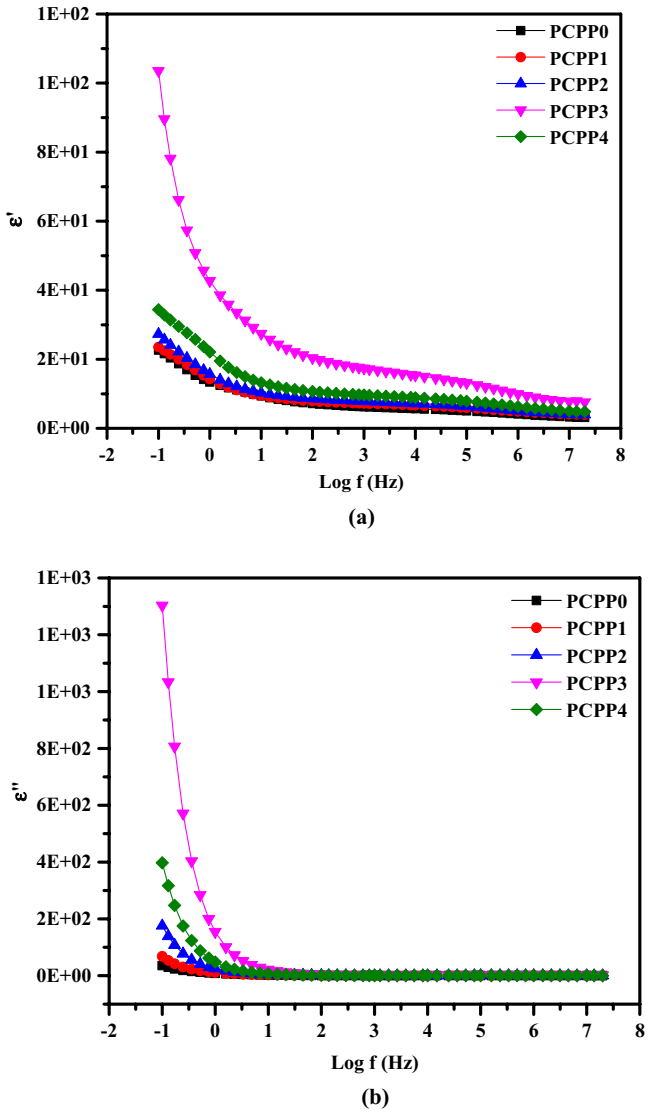

Figure 8. Frequency-dependent (**a**) real part ε′ and (**b**) imaginary part ε″ of the complex dielectric permittivity for all films at room temperature.

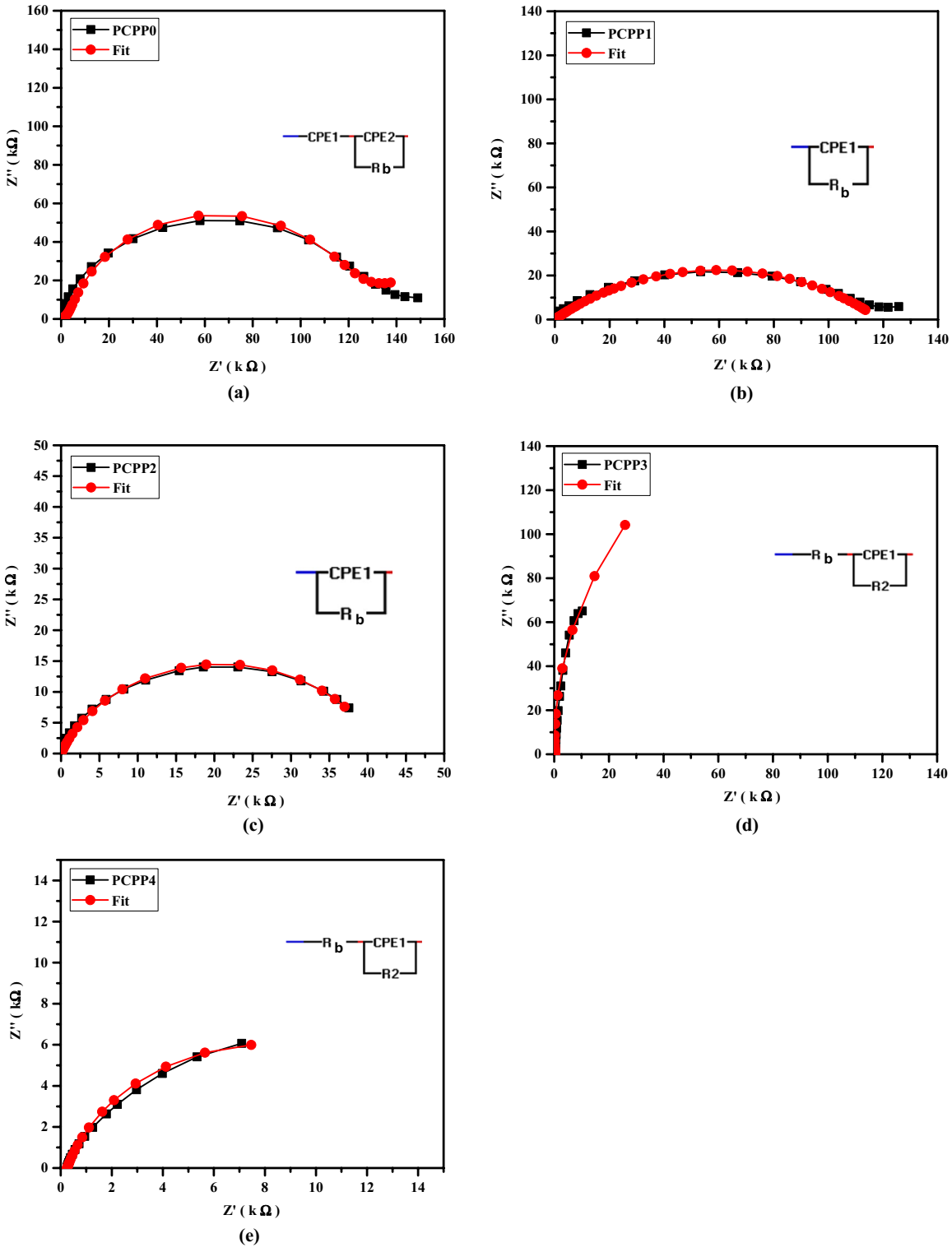

Figure 9. (**a**–**e**) Nyquist plots of the prepared nanocomposite films.

Films	Fitting parameters				
	R_b (k Ω)	Q_1 (F)	n_1	Q_2 (F)	n_2
PCPP0	142	3.3×10^{-5}	0.3	4.18×10^{-7}	0.94
PCPP1	118	6.35×10^{-7}	0.46		
PCPP2	41	8.14×10^{-6}	0.77		
PCPP3	0.450	2.48×10^{-5}	0.99		
PCPP4	0.252	6.61×10^{-5}	0.82		

Table 2. The extracted parameters of the equivalent electric circuit model.

Data availability

All data generated during this study are included in this published article.

Received: 1 October 2022; Accepted: 28 November 2022
Published online: 08 December 2022

References

1. Xue, C. *et al.* Morphology of PI–PEO block copolymers for lithium batteries. *Polymer (Guildf)* **47**, 6149–6155 (2006).
2. Wu, I.-D. & Chang, F.-C. Determination of the interaction within polyester-based solid polymer electrolyte using FTIR spectroscopy. *Polymer (Guildf)* **48**, 989–996 (2007).
3. Sedlařík, V., Saha, N., Kuřitka, I. & Sáha, P. Characterization of polymeric biocomposite based on poly(vinyl alcohol) and poly(vinyl pyrrolidone). *Polym. Compos.* **27**, 147–152 (2006).
4. Jipa, I. M. *et al.* Effect of gamma irradiation on biopolymer composite films of poly(vinyl alcohol) and bacterial cellulose. *Nucl. Instrum. Methods Phys. Res. B* **278**, 82–87 (2012).
5. Azmi, S. *et al.* Reinforcement of poly(vinyl alcohol) hydrogel with halloysite nanotubes as potential biomedical materials. *Soft Mater* **15**, 45–54 (2017).
6. Luna-Martínez, J. F. *et al.* Synthesis and optical characterization of ZnS–sodium carboxymethyl cellulose nanocomposite films. *Carbohydr. Polym.* **84**, 566–570 (2011).
7. Xiao, C. & Gao, Y. Preparation and properties of physically crosslinked sodium carboxymethylcellulose/poly(vinyl alcohol) complex hydrogels. *J. Appl. Polym. Sci.* **107**, 1568–1572 (2008).
8. Taleb, M. F. A., El-Mohdy, H. L. A. & El-Rehim, H. A. A. Radiation preparation of PVA/CMC copolymers and their application in removal of dyes. *J. Hazard Mater.* **168**, 68–75 (2009).
9. Chalmers, E., Lee, H., Zhu, C. & Liu, X. Increasing the conductivity and adhesion of polypyrrole hydrogels with electropolymerized polydopamine. *Chem. Mater.* **32**, 234–244 (2020).
10. Han, L. *et al.* Transparent, adhesive, and conductive hydrogel for soft bioelectronics based on light-transmitting polydopamine-doped polypyrrole nanofibrils. *Chem. Mater.* **30**, 5561–5572 (2018).
11. Yin, J. *et al.* Self-assembled functional components-doped conductive polypyrrole composite hydrogels with enhanced electrochemical performances. *RSC Adv.* **10**, 10546–10551 (2020).
12. Lin, Y., Zhang, H., Liao, H., Zhao, Y. & Li, K. A physically crosslinked, self-healing hydrogel electrolyte for nano-wire PANI flexible supercapacitors. *Chem. Eng. J.* **367**, 139–148 (2019).
13 Zhong, R. *et al.* Self-assembly of enzyme-like nanofibrous g-molecular hydrogel for printed flexible electrochemical sensors. *Adv. Mater.* **30**, 1706887 (2018).
14. Yang, Y., Zhao, G., Cheng, X., Deng, H. & Fu, Q. Stretchable and healable conductive elastomer based on PEDOT:PSS/natural rubber for self-powered temperature and strain sensing. *ACS Appl. Mater. Interfaces* **13**, 14599–14611 (2021).
15. Azar, M. G. *et al.* Tough and flexible conductive triple network hydrogels based on agarose/polyacrylamide/polyvinyl alcohol and poly(3,4-ethylenedioxythiophene):polystyrene sulfonate. *Polym. Int.* **70**, 1523–1533 (2021).
16. Zhang, M., Yuan, W., Yao, B., Li, C. & Shi, G. Solution-processed PEDOT:PSS/graphene composites as the electrocatalyst for oxygen reduction reaction. *ACS Appl. Mater. Interfaces* **6**, 3587–3593 (2014).
17. Su, Z. *et al.* Co-electro-deposition of the MnO_2-PEDOT:PSS nanostructured composite for high areal mass, flexible asymmetric supercapacitor devices. *J. Mater. Chem. A Mater.* **1**, 12432–12440 (2013).
18. Antiohos, D. *et al.* Compositional effects of PEDOT-PSS/single walled carbon nanotube films on supercapacitor device performance. *J. Mater. Chem.* **21**, 15987–15994 (2011).
19. Yun, D.-J. & Rhee, S.-W. Composite films of oxidized multiwall carbon nanotube and poly(3,4-ethylenedioxythiophene): Polystyrene sulfonate (PEDOT:PSS) as a contact electrode for transistor and inverter devices. *ACS Appl. Mater. Interfaces* **4**, 982–989 (2012).
20. Yeh, M. H. *et al.* A composite catalytic film of PEDOT:PSS/TiN-NPs on a flexible counter-electrode substrate for a dye-sensitized solar cell. *J. Mater. Chem.* **21**, 19021–19029 (2011).
21. Liu, N. *et al.* Electrospun PEDOT:PSS–PVA nanofiber based ultrahigh-strain sensors with controllable electrical conductivity. *J. Mater. Chem.* **21**, 18962 (2011).
22. Nikolou, M. & Malliaras, G. G. Applications of poly(3,4-ethylenedioxythiophene) doped with poly(styrene sulfonic acid) transistors in chemical and biological sensors. *Chem. Rec.* **8**, 13–22 (2008).
23. Gaabour, L. H. Effect of selenium oxide nanofiller on the structural, thermal and dielectric properties of CMC/PVP nanocomposites. *J. Market. Res.* **9**, 4319–4325 (2020).
24. Kanmani, P. & Rhim, J.-W. Properties and characterization of bionanocomposite films prepared with various biopolymers and ZnO nanoparticles. *Carbohydr. Polym.* **106**, 190–199 (2014).
25. Salim, E. Charge extraction enhancement in hybrid solar cells using n-ZnO/p-NiO nanoparticles. *J. Mater. Sci. Mater. Electron.* **32**, 28830–28839 (2021).
26. Bikiaris, D. N. & Triantafyllidis, K. S. HDPE/Cu-nanofiber nanocomposites with enhanced antibacterial and oxygen barrier properties appropriate for food packaging applications. *Mater. Lett.* **93**, 1–4 (2013).
27. Mathew, M., Sureshkumar, S. & Sandhyarani, N. Synthesis and characterization of gold–chitosan nanocomposite and application of resultant nanocomposite in sensors. *Colloids Surf. B Biointerfaces* **93**, 143–147 (2012).
28. Rhim, J. W., Wang, L. F. & Hong, S. I. Preparation and characterization of agar/silver nanoparticles composite films with antimicrobial activity. *Food Hydrocoll.* **33**, 327–335 (2013).

29. El-Nahrawy, A. M., AbouHammad, A. B., Khattab, T. A., Haroun, A. & Kamel, S. Development of electrically conductive nanocomposites from cellulose nanowhiskers, polypyrrole and silver nanoparticles assisted with Nickel(III) oxide nanoparticles. *React. Funct. Polym.* **149**, 104533 (2020).
30. Mansur, H. S., Sadahira, C. M., Souza, A. N. & Mansur, A. A. P. FTIR spectroscopy characterization of poly (vinyl alcohol) hydrogel with different hydrolysis degree and chemically crosslinked with glutaraldehyde. *Mater. Sci. Eng. C* **28**, 539–548 (2008).
31. Luo, S. *et al.* Excellent self-healing and antifogging coatings based on polyvinyl alcohol/hydrolyzed poly(styrene-co-maleic anhydride). *J. Mater. Sci.* **54**, 5961–5970 (2019).
32. Qashou, S. I., El-Zaidia, E. F. M., Darwish, A. A. A. & Hanafy, T. A. Methylsilicon phthalocyanine hydroxide doped PVA films for optoelectronic applications: FTIR spectroscopy, electrical conductivity, linear and nonlinear optical studies. *Phys. B Condens. Matter* **571**, 93–100 (2019).
33. Shi, D., Wang, F., Lan, T., Zhang, Y. & Shao, Z. Convenient fabrication of carboxymethyl cellulose electrospun nanofibers functionalized with silver nanoparticles. *Cellulose* **23**, 1899–1909 (2016).
34. Pasha, A. & Khasim, S. Highly conductive organic thin films of PEDOT–PSS:silver nanocomposite treated with PEG as a promising thermo-electric material. *J. Mater. Sci. Mater. Electron.* **31**, 9185–9195 (2020).
35. Yu, J., Gu, W., Zhao, H. & Ji, G. Lightweight, flexible and freestanding PVA/PEDOT: PSS/Ag NWs film for high-performance electromagnetic interference shielding. *Sci. China Mater.* **64**, 1723–1732 (2021).
36. Lee, J. H. *et al.* PEDOT-PSS embedded comb copolymer membranes with improved CO_2 capture. *J. Memb. Sci.* **518**, 21–30 (2016).
37. Wang, Y., Qu, Z., Wang, W. & Yu, D. PVA/CMC/PEDOT:PSS mixture hydrogels with high response and low impedance electronic signals for ECG monitoring. *Colloids Surf. B Biointerfaces* **208**, 112088 (2021).
38. Yu, J., Gu, W., Zhao, H. & Ji, G. Lightweight, flexible and freestanding PVA/PEDOT: PSS/Ag NWs film for high-performance electromagnetic interference shielding. *Sci. China Mater.* **64**, 1723–1732 (2021).
39. Jasna, M., Pushkaran, N. K., Manoj, M., Aanandan, C. K. & Jayaraj, M. K. Facile Preparation of lightweight and flexible PVA/PEDOT:PSS/MWCNT ternary composite for high-performance EMI shielding in the X-band through absorption mechanism. *J. Electron. Mater.* **49**, 1689–1701 (2020).
40. El-Bana, M. S., Mohammed, G., el Sayed, A. M. & El-Gamal, S. Preparation and characterization of PbO/carboxymethyl cellulose/polyvinylpyrrolidone nanocomposite films. *Polym. Compos.* **39**, 3712–3725 (2018).
41. Wang, X. *et al.* Enhancement of thermoelectric performance of PEDOT:PSS films by post-treatment with a superacid. *RSC Adv.* **8**, 18334–18340 (2018).
42. Rangari, V. K. *et al.* Synthesis of Ag/CNT hybrid nanoparticles and fabrication of their Nylon-6 polymer nanocomposite fibers for antimicrobial applications. *Nanotechnology* **21**, 095102 (2010).
43. Hassen, A., el Sayed, A. M., Morsi, W. M. & El-Sayed, S. Influence of Cr_2O_3 nanoparticles on the physical properties of polyvinyl alcohol. *J Appl Phys* **112**, 093525 (2012).
44. Alshehari, A. M., Salim, E. & Oraby, A. H. Structural, optical, morphological and mechanical studies of polyethylene oxide/sodium alginate blend containing multi-walled carbon nanotubes. *J. Market. Res.* **15**, 5615–5622 (2021).
45. Devi, C. U., Sharma, A. K. & Rao, V. V. R. N. Electrical and optical properties of pure and silver nitrate-doped polyvinyl alcohol films. *Mater. Lett.* **56**, 167–174 (2002).
46. Nasrallah, D. A. & Ibrahim, M. A. Enhancement of physico-chemical, optical, dielectric and antimicrobial properties of polyvinyl alcohol/carboxymethyl cellulose blend films by addition of silver doped hydroxyapatite nanoparticles. *J. Polym. Res.* **29**, 86 (2022).
47. Aziz, S. B., Abidin, Z. H. Z. & Kadir, M. F. Z. Innovative method to avoid the reduction of silver ions to silver nanoparticles. *Phys. Scr.* **90**, 035808 (2015).
48. Aziz, S. B., Abdullah, O. G. & Rasheed, M. A. A novel polymer composite with a small optical band gap: New approaches for photonics and optoelectronics. *J. Appl. Polym. Sci.* **134**, 21 (2017).
49. Bouaamlat, H. *et al.* Dielectric properties, AC conductivity, and electric modulus analysis of bulk ethylcarbazole-terphenyl. *Adv. Mater. Sci. Eng.* **2020**, 1–8 (2020).
50. Arya, A. & Sharma, A. L. Structural, electrical properties and dielectric relaxations in Na^+ -ion-conducting solid polymer electrolyte. *J. Phys. Condens. Matter* **30**, 165402 (2018).
51. Abdelrazek, E. M., Abdelghany, A. M., Tarabiah, A. E. & Zidan, H. M. AC conductivity and dielectric characteristics of PVA/PVP nanocomposite filled with MWCNTs. *J. Mater. Sci. Mater. Electron.* **30**, 15521–15533 (2019).
52. Zeyada, H. M., El-Taweel, F. M., El-Nahass, M. M. & El-Shabaan, M. M. Effect of substitution group on dielectric properties of 4H-pyrano [3, 2-c] quinoline derivatives thin films. *Chin. Phys. B* **25**, 077701 (2016).
53. Sengwa, R. J. & Choudhary, S. Dielectric and electrical properties of PEO–Al_2O_3nanocomposites. *J. Alloys Compd.* **701**, 652–659 (2017).
54. George, M., Nair, S. S., Malini, K. A., Joy, P. A. & Anantharaman, M. R. Finite size effects on the electrical properties of sol-gel synthesized $CoFe_2O_4$ powders: Deviation from Maxwell–Wagner theory and evidence of surface polarization effects. *J. Phys. D Appl. Phys.* **40**, 1593–1602 (2007).
55. Karthikeyan, A., Vinatier, P. & Levasseur, A. Study of lithium glassy solid electrolyte/electrode interface by impedance analysis. *Bull. Mater. Sci.* **23**, 179–183 (2000).
56. Khiar, A. S. A. & Arof, A. K. Conductivity studies of starch-based polymer electrolytes. *Ionics (Kiel)* **16**, 123–129 (2010).
57. Hema, M., Selvasekerapandian, S. & Hirankumar, G. Vibrational and impedance spectroscopic analysis of poly(vinyl alcohol)-based solid polymer electrolytes. *Ionics (Kiel)* **13**, 483–487 (2007).

Author contributions

E.S. planned and performed the experiments and wrote the manuscript. W.H. performed the experiments and wrote the methods. A.H.O. supervised the work and edited the manuscript. A.G.E. was also involved in the supervision.

Funding

Open access funding provided by The Science, Technology & Innovation Funding Authority (STDF) in cooperation with The Egyptian Knowledge Bank (EKB).

Competing interests

The authors declare no competing interests.

Additional information

Correspondence and requests for materials should be addressed to E.S.

Reprints and permissions information is available at www.nature.com/reprints.